Experimental cyclic behaviour of stone masonry spandrels

F. Graziotti
ROSE School, IUSS, Pavia, Italy

G. Magenes & A. Penna
University of Pavia and European Centre for Training and Research in Earthquake Engineering (EUCENTRE), Pavia, Italy

SUMMARY:
The seismic response of URM structures is influenced by the behaviour of spandrel elements, as also demonstrated by numerical simulations and post-earthquake observation. Until recently, the understanding of the seismic behaviour of these structural components was not supported by adequate experimental campaigns. Only in the last few years some experimental programs have been performed with the purpose of studying the in-plane cyclic behaviour of masonry spandrel beams, made of clay bricks or perforated blocks. The experimental study presented in this work aims at investigating the seismic behaviour of stone masonry spandrels, both in the presence or in the absence of a horizontal tensile resistant element. For this reason, an experimental apparatus was designed in order to test full-scale masonry spandrel specimens. The test setup allows to investigate the behaviour of spandrels reproducing realistic boundary conditions in the element; in particular, attention was paid to the connection between spandrel and piers.

Keywords: stone masonry, masonry spandrel, full scale test, timber lintel

1. INTRODUCTION

The term masonry spandrel (or masonry beam) defines the portion of wall that links two adjacent piers across an opening. Masonry spandrels result often damaged during a seismic event and in general they are the first structural components that crack in unreinforced masonry (URM) buildings. Spandrel elements influence significantly the force/deformation characteristics of a masonry structure due to the framing and coupling action. Recognizing that the masonry piers are the most important elements both for vertical load carrying capacity and for the resistance to seismic action, it is nevertheless not generally correct to neglect the presence of the spandrels and their role in increasing stiffness. The performance of a multi-storey wall could significantly change due to the behaviour of the spandrels. An analysis with rough assumptions regarding the contribution of spandrels may lead to either underestimate or overestimate the capacity of the structural system (Magenes and Della Fontana, 1998; Magenes, 2000; Benedetti and Magenes, 2001; Da Paré, 2011).

Figure 1.1. shows that a different degree of coupling offered by the spandrels may introduce a completely different structural behaviour in terms of shear, moment diagrams and collapse mechanism. In particular the figure shows the two extreme ideal conditions of infinitely flexible (a) and infinitely stiff (c) spandrels, corresponding to cantilever and shear-type mechanisms, respectively.

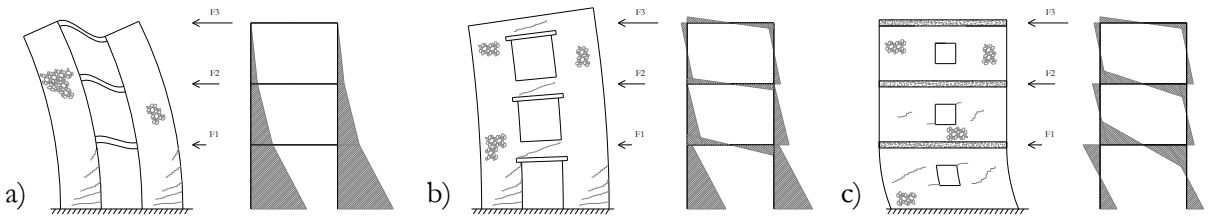

Figure 1.1. Effect of the different degree of coupling provided by the spandrels on moment distribution: weak (a), intermediate (b) and strong (c) spandrels (adapted from Tomaževič, 1999)

The most realistic situation appears to be in between these extreme conditions, as represented in the intermediate (b) configuration, in which the spandrel beams offer a limited degree of coupling to the vertical masonry piers.

Available laboratory tests on masonry buildings were mainly focused on the study of the pier element behaviour, and masonry spandrels were not studied with a sufficient detail until very recently. This may be due first of all to the fact that these structural components were considered of secondary importance and secondly to the fact that it is quite difficult to implement in the laboratory the boundary conditions to accurately reproduce the behaviour of the pier/spandrel interaction, maintaining clear static and kinematic boundary conditions.

Tests carried out in the past on spandrels were performed considering the specimen as a 90° rotated masonry pier, although this solution was not considered fully capable to replicate the actual response by the authors themselves (e.g. Genovese, 2001). The resisting mechanism of these structural components could be strongly influenced by the combination of masonry arrangement, direction of gravity and boundary conditions (e.g. effect of friction on horizontal bed-joints) at the interface between pier and spandrel. Recently, in the experimental campaigns performed at the University of Trieste (Gattesco *et al*., 2008) and at ETH Zurich (Dazio and Beyer 2010) test setups were developed allowing to recreate realistic condition for testing full-scale H shaped specimens representing a spandrel and two adjacent piers were used. At the University of Naples, Augenti et al. (2011), also, carried out tests on URM portal frames aiming to investigate the role of spandrels, considering also the effect of fiber composite strengthening. .

This paper describes the laboratory tests on two masonry spandrel specimens that were carried out at the EUCENTRE TREES Lab in 2010. In particular two stone masonry specimens were tested with a configuration that allows to control the horizontal force in the spandrel and the vertical compression in the piers. In the following pages the test setup, the mechanical and geometrical properties of the specimens and the results of the tests are described.

2. TEST SETUP

In order to realistically simulate the behaviour of the spandrels it was necessary to realize a test configuration that recreates the boundary condition in the element as if it was part of a perforated masonry wall. In the design of the test setup, a statically determined spandrel element specimen was a fundamental condition in order to have an objective measure of the axial force, shear force, and bending moment acting in the spandrel. The system is able to control each of the actions in the specimen, and it allows the shear and axial forces to be controlled independently. The static scheme of the masonry specimen is shown in Fig 2.1.

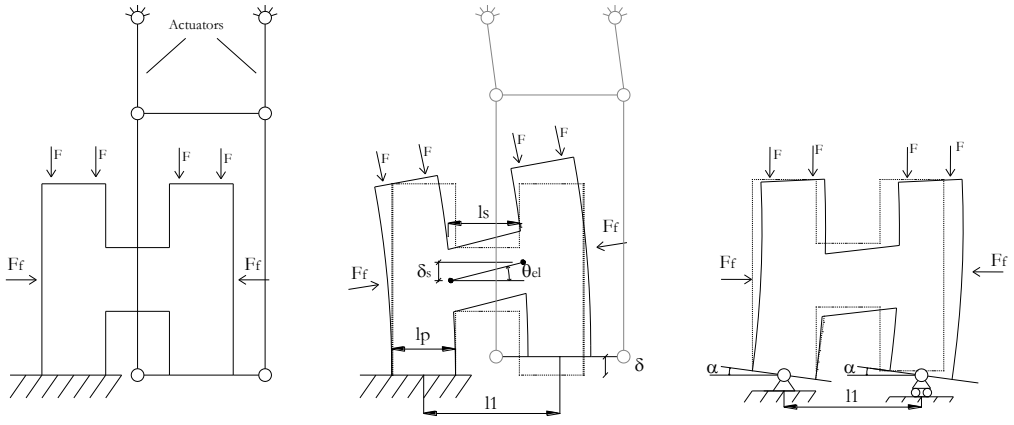

Figure 2.1. Scheme of the test setup and comparison of the deformation fields corresponding to an uplift of the right pier (centre) and a rotation of the bases of the piers (right)

The shear force in the spandrel can be easily computed as the force variation in the vertical servohydraulic actuators with respect to the initial value (accounting for the weight of the right pier and of the test equipment).

$$V_s = V_{eff} \tag{2.1}$$

$$M_{sR} + M_{sL} = V_s \cdot l_s \tag{2.2}$$

where V_s is the shear in the spandrel, V_{eff} the uplifting force in the actuators minus the weight of the pier and of the test equipment, l_s the spandrel length and M_{sL}, M_{sR} the moments in the spandrel extremities (left and right).

The horizontal displacement of the right pier is not restrained. The horizontal compression force F_f in the spandrel could be controlled by a self-equilibrated system consisting of a hydraulic jack and two external steel rods connecting the extreme ends of the H specimen. The vertical compression of the two piers was applied by one vertical hydraulic jack each, transferring the reaction of the jack to the r.c foundation of each wall by means of 4 steel rods. The compression in the piers has the double role of creating a realistic stress condition in the piers and of increasing the strength of the piers to be sure that the spandrel is the weakest part of the specimen. The rotation on the top of the two piers was not constrained. The vertical servo-hydraulic actuators were double pinned. This created a pendular system that allowed the right pier to move vertically without external horizontal restraints that could generate variation in the horizontal compression force in the spandrel. The shortening (or the elongation) of the two vertical servo-hydraulic actuators must be the same in order to impose a movement of the r.c. foundation parallel to the ground. Fig. 2.1. shows that the deformation corresponding to an uplift of the right pier, i.e. the configuration adopted in the tests (centre), is the same that would be obtained by an equal rotation of the two bases (with no restraints in horizontal direction) (right). In particular the rotation at the base of the piers, α, is given by:

$$\alpha = \arctan(\delta / l_1) = \arctan[\delta / (l_s + l_p)] \approx \delta / l_1 \tag{2.3}$$

$$\theta_{el} = \delta_s / l_f \tag{2.4}$$

with all the quantities described in Figure 2.1.

3. MECHANICAL AND GEOMETRICAL CHARACTERIZATION OF THE DOUBLE-LEAF STONE MASONRY SPECIMES

Within the framework of the RELUIS Research Program and the Eucentre Executive Project for 2005-2008, an extensive experimental campaign was planned. Its main focus is on shake table testing of three full scale prototypes of stone masonry buildings (Magenes et al., 2012). The prototypes were made of the same type of masonry of the two spandrel specimens. The experimental campaign includes a set of characterization tests to define the mechanical properties of masonry: several wall specimens were built for vertical compression, diagonal compression and in-plane shear-compression tests (Magenes et al., 2010a and 2010b).

3.1. Masonry characterization

Information on the mechanical characterization of the material and on the type of masonry used for the test is reported in Magenes et al. (2010b). Two types of test were conducted: uniaxial vertical compression and diagonal compression. Table 3.1. shows some of the most important parameters such as: masonry compressive strength f_m, masonry ultimate tensile strength f_t from diagonal compression tests, modulus of elasticity E (secant at $1/3 \cdot f_m$) and shear modulus G (secant at $1/3 \cdot f_t$).

3.2. Mortar characterization

To satisfy the requirement of having a mortar as consistent as possible with that of historical buildings, it was necessary to derive an appositely produced type of lime mortar. Tests on twelve mortar specimens were carried out after more than 28 days, according UNI EN 1015-11 code (see Table 3.1.)

Table 3.1. Summary of the results of experimental wall compression tests (Magenes et al., 2010) and summary of the results of mortar compressive and flexural strength tests

	Masonry				**Mortar**	
[MPa]	f_m	**E**	f_t	**G**	f_c	f_t
Mean	3.28	2550	0.137	840	1.7	0.44
St. Dev.	0.26	345	0.031	125	0.28	0.11
C.o.v.	8%	13.5%	21.8%	14.8%	17%	26%

3.3. Geometrical properties of the specimens

Two full-scale double-leaf stone spandrel specimens were tested. They were made up of two piers and a spandrel supported by a timber lintel. The difference between the two tests was the presence of a horizontal compression in the second specimen (S2), while the first one (S1) had zero compression. The presence of a horizontal compression in a real spandrel may be due for instance to the presence of horizontal steel ties, typically positioned at the floor levels. The dimensions of the two specimens were identical and they are reported in Fig. 3.1(left).

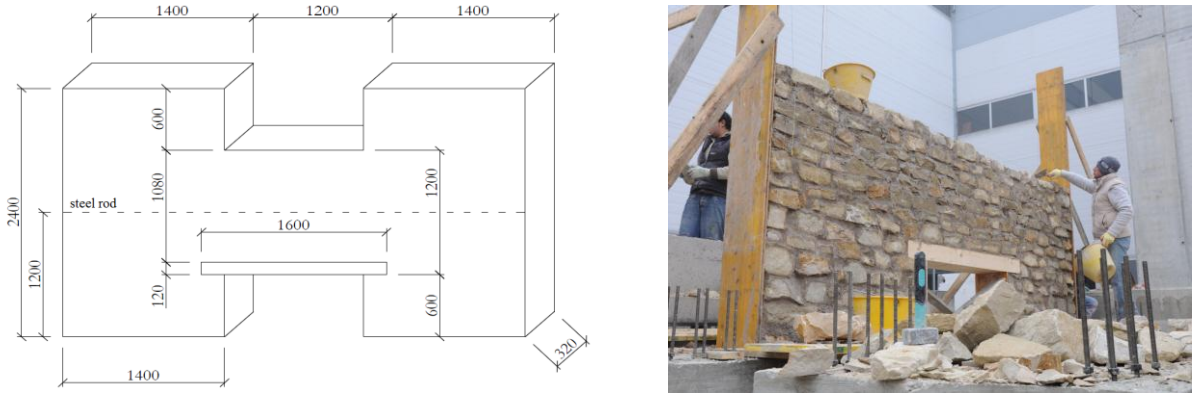

Figure 3.1. Dimensions of the two double-leaf stone masonry specimen [mm] (left) and picture taken during the construction on the first specimen (right)

4. INSTRUMENTATION OF THE SPECIMENS

Different global and local deformation quantities as well as actuator forces were measured during testing. In particular deformations were measured by means of two independent systems: traditional electromechanical displacement transducers and an optical system consisting in a grid of reflector markers monitored by high definition cameras.

4.1. Actuators force transducers

Load cells were used to measure the force given by the two vertical actuators. The forces in the other hydraulic jacks were measured by means of digital manometers. Two of them were measuring the pressure in the vertical jack (compression in the piers) and the other one in the jack that induces tension to the spandrel's horizontal rods (only in the second test).

4.2. Displacement transducers (potentiometers)

Linear potentiometer displacement transducers were placed in convenient positions on the specimen, in order to measure differential displacements. Fifty linear displacement transducers with ball tip and with cylindrical case were used to measure the relative displacements between the two ends of the instruments, allowing the average deformation along the instrument length to be derived.

4.3. Advanced optical acquisition of absolute displacements

Information about the displacement response of the structures during the tests was provided by video acquisition with two infrared High Definition cameras. The motion was detected through reflector markers, allowing the evaluation of displacements in the vertical plane framed by the cameras.

5. TEST PROCEDURE

The cyclic tests on double-leaf stone wall were carried out in displacement control. The horizontal compressive force in the spandrel was zero for S1 and 75 kN, 38kN, 19kN in the different phases of the test on S2. The vertical force in the piers was 75 kN in both cases, which is equivalent to a compression of 0.17 MPa. Following the specifications above mentioned the base of the right pier was uplifted generating a drift in the spandrel element. The nominal element drift it's so defined as:

$$\theta_n = \delta / l_f \tag{5.1}$$

with all the quantities defined in Fig. 2.1.
Each step of the test consisted of three loading cycles at a given drift level, with progressively increasing drift target levels. Each cycle took approximately 120 seconds; the maximum velocity was of 0.5 mm/s.

5.1. Loading history applied to the first spandrel specimen (S1, F_f=0)

In the test of specimen S1 there was no horizontal force applied to the spandrel, as there was no tie rod installed. A problem in the support of the mobile pier forced to begin the test with a monotonic ramp up to 6 mm of displacement (θ_n = 0.5%). After that, complete loading cycles were performed reaching the specimen rupture at 18 mm (θ_n = 1.5%). The loading history followed during the test on the 1st specimen is summarized in Fig. 5.1 (left).

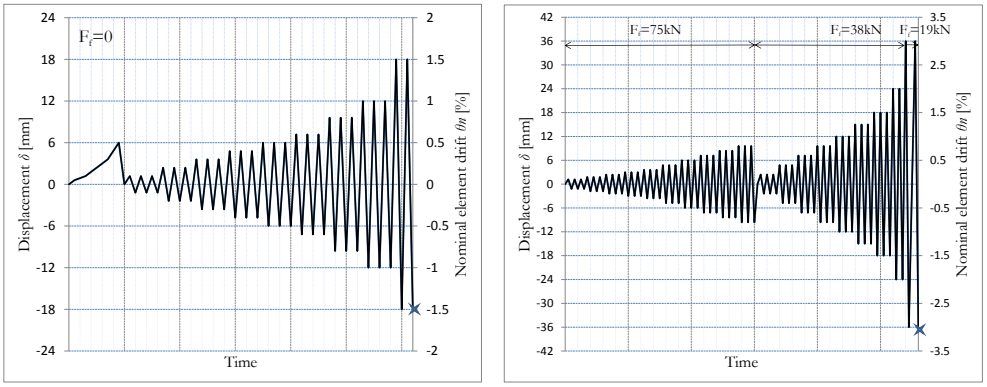

Figure 5.1. Loading histories applied during the tests on the two specimens (S1 left, and S2 right)

5.2. Loading history applied to the second spandrel specimen (S2, F_f=0)

In the test of specimen S2 the horizontal compressive force in the spandrel was constant in each cycle. In particular 3 values were used. 75 kN up to a drift of 9.6 mm (θ_n = 0.8%), 38 kN up to 36 mm (θ_n =

3%) and 19 kN just for the last 3% drift cycle. The loading history followed during the test on the 2nd specimen is summarized in Fig. 5.1 (right).

6. TEST RESULTS

6.1. Test on the first specimen (S1, $F_f = 0$)

6.1.1. Test observations

A representation of the evolution of the crack pattern observed for the first specimen is reported in the left side of Fig. 6.2. The first crack occurred at θ_n = 0.15% (step M4). This vertical flexural crack started in the upper right corner of the spandrel and developed for a total length of about 40 cm. The test continued with a monotonic ramp and at θ_n = 0.2% (step M5) a similar crack appeared starting from the opposite lower left corner, near the timber lintel. This monotonic ramp ended at a displacement of 6 mm corresponding to a nominal drift (θ_n) of 0.5%. At that stage the flexural cracks on the interfaces between spandrel and piers became longer (approximately 700 mm). This indicates that the compressed strut in the spandrel (from top left to bottom right) had a very small depth. At this stage the wood lintel appeared to be well bonded to the piers and no horizontal relative displacement between the two components was noticed. After this stage the cyclic test began.

Figure 6.1. View of the entire specimen at C15 (θ_n = 1.5%) (left) and crack pattern of spandrel at C10 (θ_n = 0.6%) (right)

The first cracks of the cyclic test were induced by flexure due to the downward movement of the right pier and occurred at step C3 (θ_n = -0.1%). The first visible sliding of the lintel on the piers took place during step C7 (θ_n = 0.3%). The left part of the lintel was debonded from the pier due to the bending moment in the spandrel element; during the uplift of the right pier that part of the lintel works as a tensile strut. At this drift the friction between masonry and lintel reached its limit, providing the maximum resisting moment of the element. Continuing the test, the spandrel element showed a "rocking" behaviour. No new cracks appeared. During step C8 (θ_n = 0.4%) the cracks on the two interfaces opened and closed under cycle reversal allowing rigid rotations of the spandrel. During step C10 (θ_n = 0.6%) these cracks were opened more than 10 mm and, at the end of the cycles, a considerable residual crack width remained as shown in Fig. 6.1 (right). The distance between the piers increased at every cycle, due to the absence of a horizontal restoring force. In particular, the final relative displacements of the lintel (after the test C15, θ_n = 1.5%) were 3.8 cm on the left and 1.8 cm on the right (Fig. 6.1). It was not easy to detect a real qualitative "collapse" point. With this crack configuration, the spandrel element would have been able to "couple" the piers for higher drifts, thanks to the presence of the wooden lintel.

6.1.2. Deformation field

The optical data acquisition allowed to compute the position of the markers continuously during the test. The right part of Fig 6.2 shows the undeformed and deformed grid of the specimen subjected to a drift θ_n = -0.8% (amplified by a factor of 20). It is possible to notice that all the deformations are

concentrated in the interfaces between piers and spandrel. The moderate coupling effect given by the spandrel is not sufficient to deform in an appreciable way the piers that simply increase their relative distance.

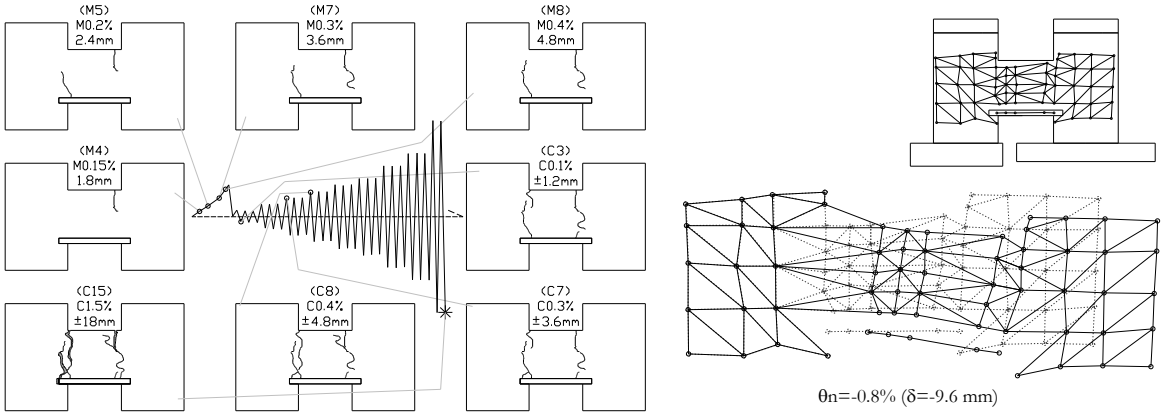

Figure 6.2. Evolution of the crack pattern observed during the first test (left), and deformation field during a negative load cycle (scale factor: 20) (right)

6.1.3. Force-displacement behaviour

Fig. 6.3. compares the spandrel shear force with 3 quantities: the base displacement δ, the element drift θ_{el} and the base equivalent rotation α (see Fig. 2.1., Eqn. 2.3 and 2.4). The force is calculated from the reading of two load cells in the vertical actuators. The maximum shear force reached during the test was about 30 kN both for positive and negative loading. It occurred at a drift θ_{el} of about 1.5‰ ($\delta \approx$ 2mm). The positive maximum shear was reached under the monotonic loading; a slightly lower value of shear was attained in the negative direction. A considerable drop in stiffness and shear force was measured during the cycles of reloading up to a positive displacement δ of 5 mm. In particular the decrease of the maximum positive peak shear force was about 30% (from 32 kN to 20 kN). The envelope of the maximum shear force dropped down to about 15 kN starting from an element drift θ_{el} of 0.5%. Looking at the crack pattern evolution it is possible to notice that, from this point, the spandrel exhibited a "rocking" mechanism, with two main open cracks along the whole height of the spandrel. This phenomenon happened in conjunction with the horizontal movement of the timber lintel relatively to the stone masonry of the pier. Then the envelope of the maximum shear force remains almost constant up to the end of the test.

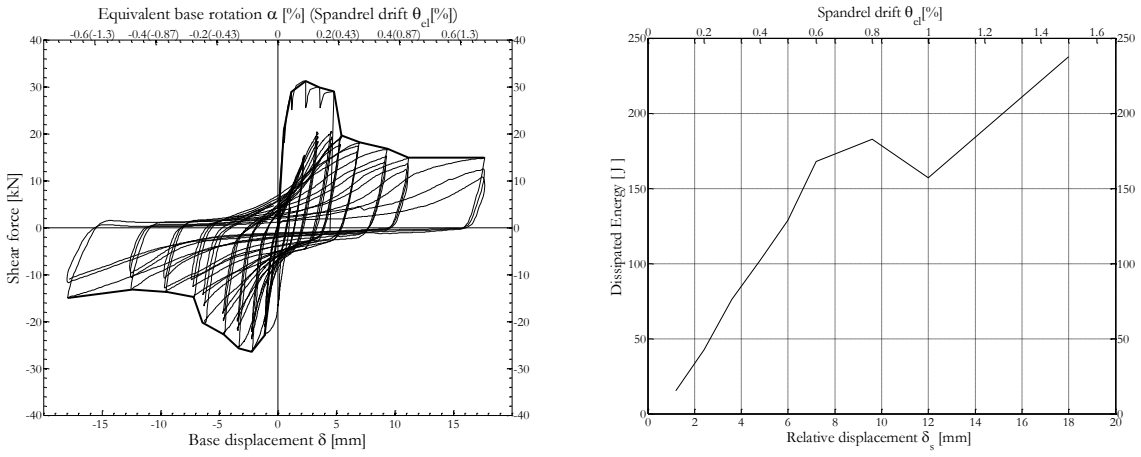

Figure 6.3. Force-displacement δ, force-eq. base rotation α and force-drift θ_{el} cycles for S1 (left); Dissipated energy per cycle vs. rel. displacement δ_s and spandrel drift θ_{el} for S1 (right)

6.2. Test on the second specimen (S2, $F_f \neq 0$)

6.2.1. Test observations

A representation of the evolution of the crack pattern observed on the second specimen is reported in

Fig. 6.5 (left). The test started with a horizontal compression of 75 kN, equivalent to a stress σ_h of 0.23 MPa. The first cracks were observed at step C6_75 (θ_n = 0.25%). A vertical small cracking in the centre of the panel (one stone layer high) and a flexural crack in the left pier starting from the left end of the timber lintel were observed. Another crack appeared at C11 (θ_n = 0.7%) in the right pier. The crack was similar to the one observed in the other pier. This indicated that the piers were cracking before the spandrel. In order to decrease the resistance of the spandrel, the horizontal compression was reduced by half (down to 38 kN, corresponding to σ_h = 0.11 MPa). The first cracks of this configuration were diagonal shear cracks and they were observed in the spandrel. In particular, during the positive displacement C13_38 (θ_n =1%) a diagonal crack spread from top left corner to the centre of the panel. Reversing the load, a shear crack propagated along the whole diagonal from the top right corner to the bottom left one. The cracks closed at the end of the cycles due to the compressive horizontal force. The positive displacement during C14_38 (θ_n =1.25%) caused the formation of a diagonal crack from the centre of the panel to the bottom right of the spandrel. During the cycles C15_38 (θ_n =1.5%) other diffused cracks appeared in the spandrel. In particular the most relevant one was a fracture similar and parallel to the crack formed in C14_38. The last cycles with new cracks forming were C17_38 (θ_n =2%), with the development of diagonal cracks near the left corners.

Figure 6.4. View of the second specimen at C19_38 (θ_n = 3%) on the left and close view of the crack pattern of the spandrel at the end of the test S2 on the right.

Two C19 (θ_n =3%) cycles were conducted at two different horizontal force levels: 38 kN and 19 kN.

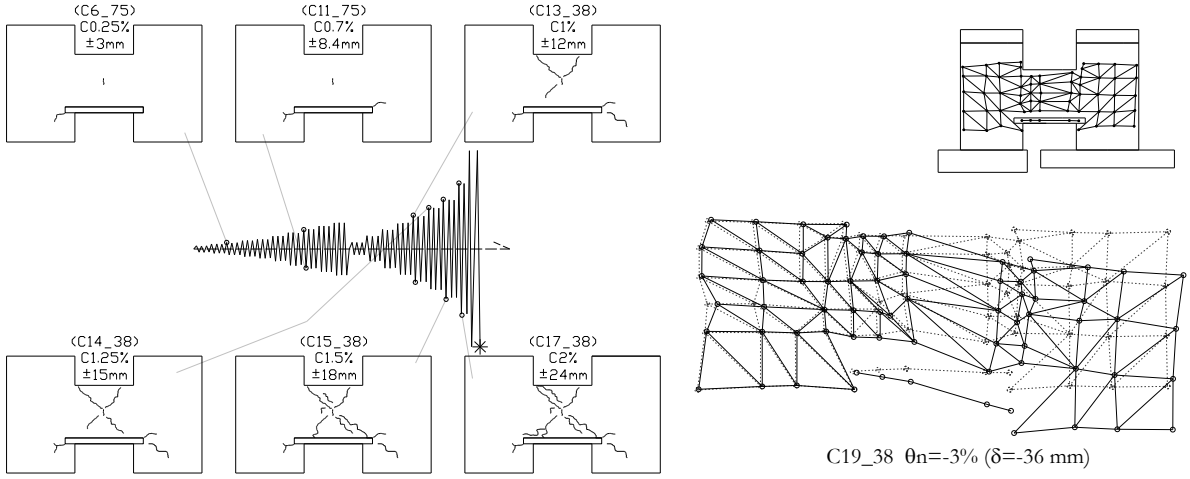

Figure 6.5. Evolution of the crack pattern observed during the second test (left), and deformation field during a negative load cycle (scale factor: 10) (right)

6.2.2. Deformation field

The right part of Fig. 6.5 shows the undeformed and deformed grid of the specimen subject to a drift θ_n = -3% (amplified by a factor 10). It is possible to notice that the deformations are spread in the spandrel element and no more concentrated in the interfaces between piers and spandrel. The stronger

coupling effect given by the spandrel was sufficient in this case to deform in an appreciable way the piers.

6.2.3. Force-displacement behaviour

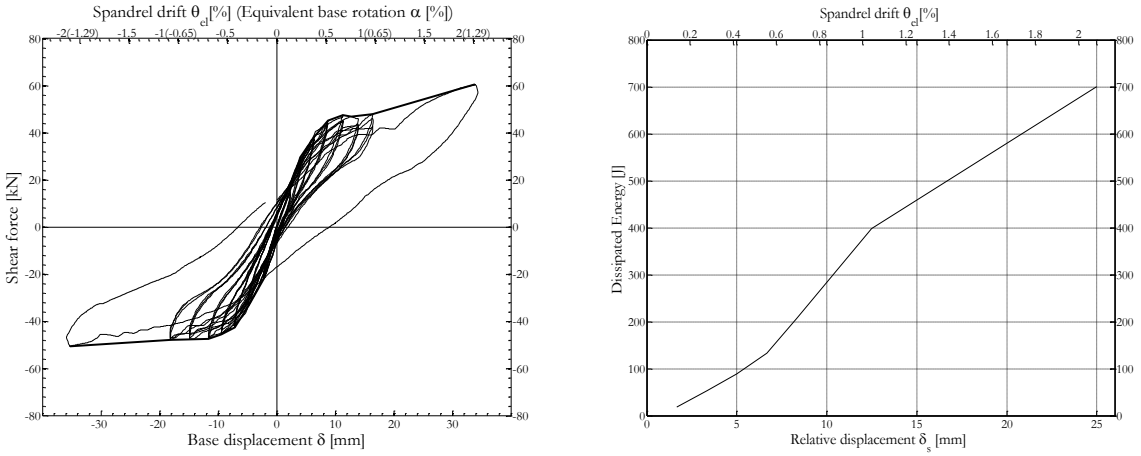

Figure 6.6. Force-displacement δ, force-eq. base rotation α and force-drift θ_{el} cycles for S2 (with F_f = 38 kN left); dissipated energy per cycle vs. rel. displacement δ_s and spandrel drift θ_{el} for S2 (right)

The maximum shear force reached during the test was about 60 kN for both positive and negative loading (F_f = 38 kN). It occurred at a drift θ_{el} of about ±2.1% (nominal drift θ_n =±3%, spandrel relative displacement $\delta_s \approx$ ±25mm, base displacement δ = ±36mm). In this test the approximation $\delta \approx \delta_s$, was not valid anymore because the piers are participating to the total specimen deformation with a rotation, and hence $\theta_{el} < \theta_n$. The observed behaviour is close to elasto-plastic, with a well-defined "yielding" point. The plastic behaviour characterizes the element after a $\theta_{el} \approx 0.5\%$, up to the final imposed drift with no softening. Looking at the crack pattern evolution it is possible to observe that the elastic behaviour ends as soon as the first small vertical crack appears in the centre of the panel, i.e. during the test C6_75 (θ_n = 0.25%).

6.3. Comparison of the results of the two tests

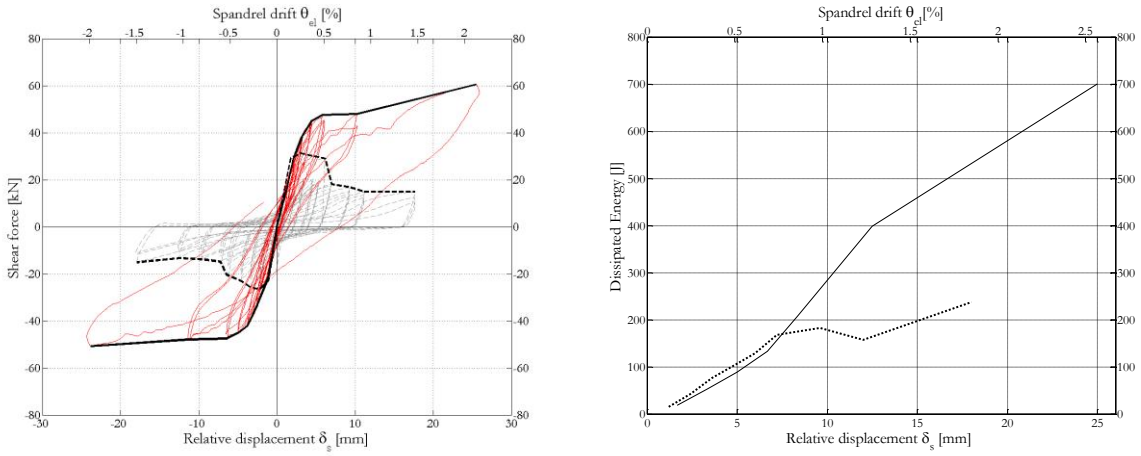

Figure 6.7. Comparison between force-rel. displacement δ_s cycles (S1, dashed - S2, solid) (left); dissipated energy per cycle vs. rel. displacement δ_s (S1, dashed - S2, solid) (right)

The main difference between tests S1 and S2 was in the failure mechanism: a flexure/rocking with added friction of the lintel in S1, a shear failure in S2. This influenced the hysteretic behaviour characterized by higher strength and small residual crack widths in case of horizontal compression

(limited damage for lower drift values), low strength and large residual cracks in case of absence of compression. Comparing the two curves it also is evident that the horizontal compression increased strength and strain capacity as well. In particular the presence of a horizontal compression of 38 kN amplified the maximum shear strength from 30kN to approximately 50 kN (plus 67%). It is difficult to directly compare the deformation capacity because the behaviour of the two specimens was completely different and a complete collapse condition was not reached in neither test. The initial stiffness did not result significantly influenced by the presence of the horizontal compression. Fig. 6.7. (right) shows that that for θ_{el} higher than 0.6% the presence of has a beneficial effect on the dissipation of energy.

7. CONCLUSIONS

The experimental study presented in this work aims at investigating the seismic behaviour of stone masonry spandrels, both in the presence and in the absence of a horizontal tie rod. For this reason an experimental apparatus was designed in order to test full-scale masonry spandrel specimens. The test setup allows to investigate the behaviour of spandrels recreating representative and controlled boundary conditions in the element. Quasi-static cyclic tests were performed in displacement control on double leaf stone masonry specimens. Studying the results of the tested specimens it is possible to observe that the masonry spandrels maintain a non-negligible resistance and dissipative capacity even after their cracking; this due to the activation of friction mechanism in the interfaces between spandrel and piers. This behaviour is possible thanks to the presence of a well anchored timber lintel that supports the spandrel even after the formation of large cracks. The experimental campaign will continue in the future with new tests, in particular with different specimen dimensions and levels of horizontal compression.

ACKNOWLEDGEMENTS

The research project was funded by the Italian Department of Civil Protection through the 2005-2008 Reluis Project. The authors would also like to thank the EUCENTRE TREES Lab and ITC service, dr. A. Galasco who provided valuable help, and Tassullo SpA for providing the lime mortar.

REFERENCES

Augenti, N., Parisi, F., Prota, A., Manfredi, G. (2011). In-plane lateral response of a full-scale masonry sub-assemblage with and without an inorganic matrix-grid strengthening system. *Journal of Composites for Construction* 15:4, 578-590.

Da Paré, M. (2011). The role of spandrel beams on the seismic response of masonry buildings, *MSc Dissertation, MEEES-ROSE School*, IUSS Pavia.

Dazio, A., Beyer, K. (2010). Seismic behaviour of different types of masonry spandrles, *14th European Conference on Eathquake Engineering*, Ohrid, FYROM, 30 August - 3 September 2010.

EN 1015-11:(1999). Methods of test for mortar for masonry - Determination of flexural and compressive strentgth of hardened mortar.

Gattesco, N., Clemente I., Macorini L., Noè S. (2008). Experimental investigation of the behaviour of spandrels in ancient masonry buildings, *Proc. of the 14th WCEE*, Beijing, China.

Genovese, C. (2001). Analisi di comportamento sotto sisma di strutture murarie con modelli funzionali. *Tesi di dottorato in ingegneria civile*, Politecnico di Torino. (Italian)

Magenes, G., Della Fontana, A. (1998). Simplified non-linear seismic analysis of masonry buildings, *Proc. of the British Masonry Soc.*, n. 8, pp.190-195.

Magenes, G. (2000). A method for pushover analysis in seismic assessment of masonry buildings, *12th World Conference on Earthquake Engineering*, Auckland, New Zealand, January 30-February 4, (CD-ROM).

Magenes, G., Penna, A., Galasco, A., Da Paré, M. (2010a). In-plane cyclic shear tests of undressed double-leaf stone masonry panels, *Proc. 8th International Masonry Conference*, pap. N. 216, Dresden, Germany.

Magenes, G., Penna, A., Galasco, A., Rota, M. (2010b). Experimental characterisation of stone masonry mechanical properties, *Proc. 8th International Masonry Conference*, pap. N. 217, Dresden, Germany.

Magenes, G., Penna, A., Rota, M., Galasco, A., Senaldi, I. (2012). Shaking table test of a full scale stone masonry building with stiffened floor and roof diaphragms. *Proc. of the 15th WCEE*, Lisbon.

Magenes, G., Penna, A., Graziotti, F. (2012). Quasi-Static Cyclic Testing of Full-Scale Stone Masonry Spandrels, *IUSS Press*, Pavia. (in press)

Tomaževič, M. (1999). Earthquake-resistant design of masonry buildings, Imperial college press London.